

## Accurate location and focal mechanism of small earthquakes near Idukki Reservoir, Kerala: implication for earthquake genesis

Utpal Saikia<sup>1,\*</sup>, S. S. Rai<sup>1</sup>, M. Subrahmanyam<sup>2</sup>,  
Satyajit Dutta<sup>1</sup>, Somasish Bose<sup>1</sup>,  
Kajaljyoti Borah<sup>1</sup> and Rishikesh Meena<sup>1</sup>

<sup>1</sup>CSIR-National Geophysical Research Institute,  
Hyderabad 500 007, India

<sup>2</sup>Department of Geophysics, Andhra University,  
Visakhapatnam 530 003, India

Earthquake waveform from a new temporary network of 21 seismic stations in South India has been used to significantly improve the detection threshold and parameters of small earthquakes near Idukki Reservoir, Kerala. We present here precise location of 16 earthquakes in this region with a local magnitude of 1.5–3.6 and focal depth 7.2–9.9 km. Fault plane solutions of the selected best six earthquakes show strike-slip faulting and right lateral movement. Reservoir loading usually leads to generation of stress and therefore earthquakes in the shallow depth (< 5 km), that are absent in the region of Idukki Reservoir. Recorded earthquakes are confined to a NW–SE trending fault close to Karur–Kambam–Painavu–Trichur (KKPT) shear zone. These observations suggest that the earthquakes in Idukki region are tectonic in nature and have no linkage with the reservoir.

**Keywords:** Earthquake location, fault plane solution, reservoir, tectonics.

As a part of India Deep Earth Imaging Experiment (INDEX)<sup>1</sup>, we operated a network of 21 broadband seismographs during January 2011–March 2012 in the South Indian states of Tamil Nadu and Kerala to map the seismic pattern and image the deep structure of the region (Figure 1). In this low strain ( $10^{-12}$  to  $10^{-13}$ /year) region<sup>2</sup>, our instruments recorded a number of small earthquakes near the Idukki Reservoir (9°50'N; 76°58.5'E) approximately 120 km east of Cochin, across the Periyar River in Kerala. The occurrence of recent seismic activity near the Idukki Reservoir has been earlier reported by Rajendran *et al.*<sup>3</sup>. However, due to inadequate instrumental data, they could not provide precise epicentre location, focal depth and magnitude of these events. Idukki is one of the highest arch dams in Asia (169 m), which has been functional since October 1975. Historically, the Kerala region has witnessed several small to moderate intensity earthquakes<sup>4,5</sup>. These include ( $M < 5$ ) the 1988 Idukki<sup>6,7</sup>, the 1994 Wadakachery<sup>8</sup> and the twin events of 2000 and 2001 at Erattupeta/Pala<sup>9,10</sup>. The low-gain seismic network

in Idukki region operating since 1971, has recorded a significant number of earthquakes<sup>7</sup>. Some of these earthquakes ( $M \leq 3.5$ ) during 1977 and 1983 occurred near the Idukki Reservoir, and were considered as reservoir induced<sup>11</sup>. Alternate view attributed these earthquakes to reactivation of pre-existing NW–SE trending faults in the region<sup>12,13</sup>. As most of the earthquakes are small, the quality and number of waveform records are poor and inadequate. As a consequence, the earthquake parameters could not be accurately determined. In this communication, we present precise hypocentre location, and focal mechanism of the earthquakes that occurred during the operational period, and discuss the possible linkage of these earthquakes to the surface geological features near the reservoir.

The Idukki Reservoir is situated in the southern part of the Western Ghats hill ranges, which run parallel to the west coast of India. Figure 1 shows the major regional structure of southern India, geologically known as Southern Granulite Terrain (SGT). The terrain is dissected by the well-mapped Moyar and Bhavani shear zones

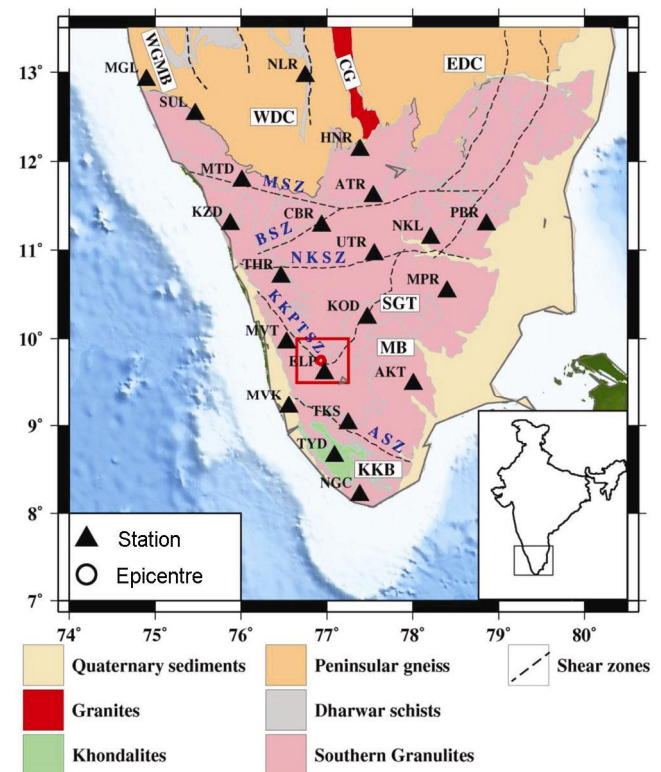


**Figure 1.** Tectonic map of the South Indian Shield showing major geological terrain, viz. EDC, Eastern Dharwar Craton; WDC, Western Dharwar Craton; SGT, Southern Granulite Terrain; CG, Closest Granite; MSZ, Moyar Shear Zone; BSZ, Bhavani Shear Zone; NKSZ, Noyil Kaveri Shear Zone; ASZ, Achankovil Shear Zone; KKPT, Karur–Kambam–Painavu–Trichur Shear Zone; MB, Madurai Block; KKB, Kerala Khondalite Belt. The rectangle indicates the area shown in Figure 2. The seismic stations used in this study (2011–2012) are shown as black triangles. The three-letter code for each station is shown and the red circle represents the location of earthquakes.

\*For correspondence. (e-mail: ngriutpal@gmail.com)

**Table 1.** Operational details of the South India seismic network

Station code	Latitude	Longitude	Elevation	Operational period
AKT	09.480	78.007	98	01/2011–04/2012
ATR	11.604	77.540	274	05/2011–04/2012
CBR	11.273	76.937	348	04/2011–05/2011
ELP	09.600	76.970	1116	05/2011–04/2012
HNR	12.126	77.385	594	02/2011–04/2012
KOD	10.230	77.470	2339	04/2010–04/2012
KZD	11.291	75.874	39	04/2010–04/2012
MGL	12.912	74.899	99	02/2009–08/2011
MPR	10.530	78.398	212	01/2011–04/2012
MTD	11.777	76.010	753	02/2009–08/2011
MVK	09.211	76.558	14	01/2011–04/2012
MVT	09.950	76.531	151	02/2011–04/2012
NGC	08.204	77.382	49	01/2011–04/2012
NKL	11.136	78.210	163	04/2010–05/2011
NLR	12.954	76.749	789	02/2009–08/2011
PBR	11.286	78.858	130	04/2011–04/2012
SUL	12.528	75.467	107	01/2011–08/2011
THR	10.697	76.465	61	02/2011–04/2012
TKS	09.023	77.246	215	01/2011–04/2012
TYD	08.650	77.090	153	05/2011–04/2012
UTR	10.950	77.540	265	05/2011–04/2012

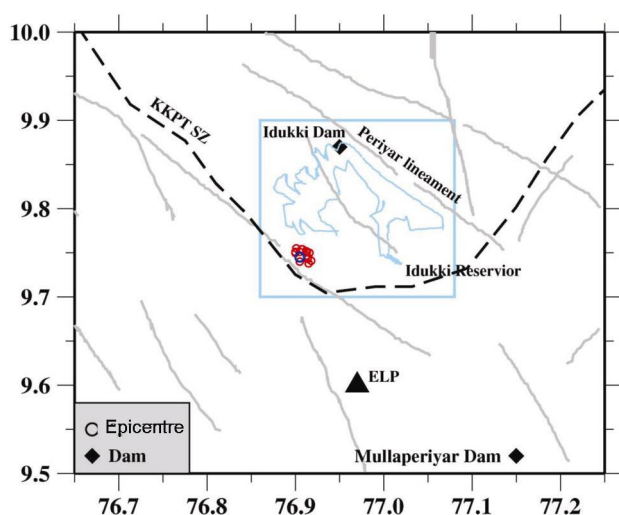


**Figure 2.** Area around the Idukki Reservoir showing faults and lineaments (from Rajendran *et al.*<sup>5</sup>). The circle represents the earthquake location in this region during July 2011–March 2012. The blue circle represents the main-event ( $M_L = 3.6$ ) and the remaining events are shown by red circles. The Karur–Kamabm–Painavu–Trichur shear zone (KKPT SZ) is shown by solid dotted line. Black triangle represents the seismic station; the ELP seismic station is the nearest one from the study area. The Idukki Reservoir is also shown. The black diamond represents the location of the dam.

(MSZ/BSZ) in the north and the Noyil–Kaveri (NKSZ) and Karur–Kambam–Painavu–Trichur (KKPT) shear zones in the south. To the south of NKSZ is the Pan-African terrain of South India comprising the northern Madurai Block (MB) and southern Kerala Khondalite Belt (KKB). The primary rock types of Idukki region

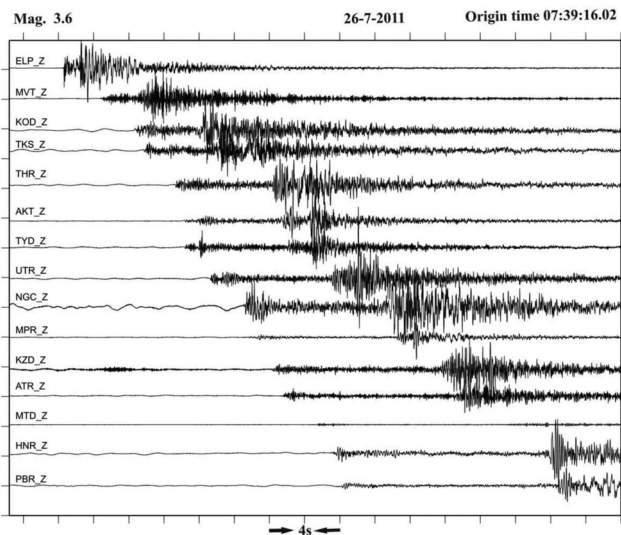
include charnockite and khondalite and gneisses. The dominant tectonic features are NW–SE trending Periyar River lineament and KKPT shear zone<sup>14,15</sup> (Figure 2). These two prominent lineaments in this region have dextral (right lateral) strike-slip components.

We deployed a temporary network of 21 digital broadband seismic stations in the region during January 2011–March 2012 (Figure 1). Station parameters are listed in Table 1. These stations are equipped with Guralp CMG-3T/ESP broadband sensors and 24-bit REFTEK (RT 130/01) data recorders with 4 GB swappable hard disk and GPS. All the stations are operated in continuous mode and waveforms recorded at a rate of 50 samples/sec.

In order to detect and extract the local earthquakes, we manually examined the continuous waveforms on a minimum of three representative stations in this region to prepare a local earthquake timing list using the REFTEK utility software, RTVIEW. This list was then used to select the seismogram time series for all other stations. Finally, we made an event-wise list of stations that recorded earthquake waveform with good signal-to-noise ratio (S/N) and clear *P*-phase. The recorded seismograms are corrected for the instrument response. We performed *P*- and *S*-phase picking using the earthquake analysis software SEISAN<sup>16</sup>. Depending on the clarity of phases, we assigned a time uncertainty of 0.05–0.50 sec for *P*-arrivals and 0.1–1.5 sec for *S*-arrivals. Arrival times are manually picked on the unfiltered seismograms to avoid phase effects. *P*-waves are picked on the vertical component and *S*-waves on one of the horizontal components. To give an idea of data quality, Figure 3 presents vertical component of seismograms for an earthquake recorded by the network.

**Table 2.** List of earthquakes in the vicinity of Idukki Reservoir recorded during 26 July 2011 to 18 March 2012 by the network of digital seismic stations

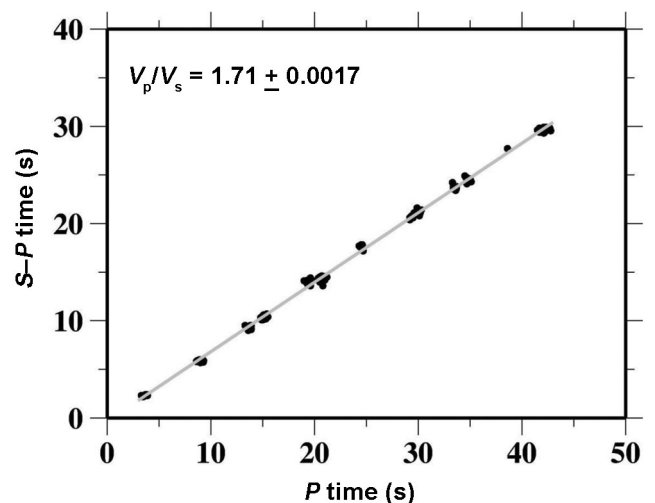
Date	UTC (time)	Latitude	Longitude	Depth	Magnitude ( $M_L$ )
26/07/2011	07:39:16.02	09.745	76.905	9.7	3.6
26/07/2011	08:45:55.52	09.752	76.912	9.9	2.9
26/07/2011	10:56:43.21	09.754	76.908	9.4	2.4
26/07/2011	18:32:03.80	09.755	76.901	9.8	1.5
23/08/2011	13:57:49.29	09.740	76.905	9.1	1.6
17/09/2011	22:26:24.40	09.750	76.916	8.9	2.0
18/09/2011	00:59:07.38	09.751	76.900	9.1	2.1
02/10/2011	21:23:12.05	09.747	76.913	9.1	1.9
07/10/2011	21:46:38.59	09.743	76.914	9.5	1.9
02/11/2011	04:53:13.47	09.744	76.914	8.9	2.2
17/11/2011	23:57:57.15	09.741	76.918	9.7	2.6
18/11/2011	00:15:38.58	09.738	76.915	9.8	3.2
25/11/2011	21:44:58.34	09.751	76.913	8.8	2.9
10/12/2011	10:11:16.72	09.754	76.907	9.9	2.0
04/03/2012	18:47:45.08	09.754	76.908	8.1	1.5
18/03/2012	19:53:23.15	09.751	76.905	7.2	2.0

**Figure 3.** Vertical component of the seismograms showing an example of one event (lat. 09.745°N, long. 76.905°E) that occurred on 26 July 2011. The three-letter code name of each station is also shown. The origin time and local magnitude of this event are 07:39:16.02 and 3.6, it was recorded in 21 stations. Here we show trace of vertical components for 15 stations.

Earthquakes (Table 2) with a minimum of 12  $P$ - and 10  $S$ -arrivals are selected for their hypocentre location using the program HYPOCENTER<sup>17</sup>. Precision of hypocentre determination depends on the distribution of the recording stations and the velocity structure between source and stations. Preliminary crustal velocity model (Table 3) used for hypocentre location is a simplified version of the initial result of inversion from receiver function studies at the stations of our network (Ritima Das, pers. commun.). The average  $V_p/V_s$  ratio of  $1.71 \pm 0.0017$  is computed from the Wadati plot using arrival time of the  $P$ -wave and  $S-P$  time (Figure 4). The azimuthal gap for these earthquakes is in the range 120°–125°. The rms time residuals,

**Table 3.** Crustal velocity model used for earthquake location

Depth (km)	$V_p$ (km/s)	$V_p/V_s$
0.0	5.80	1.73
6.0	6.10	1.73
20.0	6.54	1.73
40.0	7.52	1.73

**Figure 4.** Linear fit of  $S-P$  time versus  $P$ -travel time to compute  $V_p/V_s$  ratio (1.71) with a standard deviation of 0.0017.

focal depth along with detailed error statistics for epicentre ( $H$ ), focal depth ( $Z$ ) and rms time residuals ( $s$ ) for all the 16 earthquakes are shown in Figure 5. Errors in epicentre, focal depth and time residual vary in the ranges 0.8–2.2 km, 1.5–2.5 km and 0.10–0.20 sec respectively. Focal depths of these earthquakes are well constrained between 7.2 and 9.9 km. Details of these earthquakes are listed in Table 2 and epicentres are shown in Figure 2

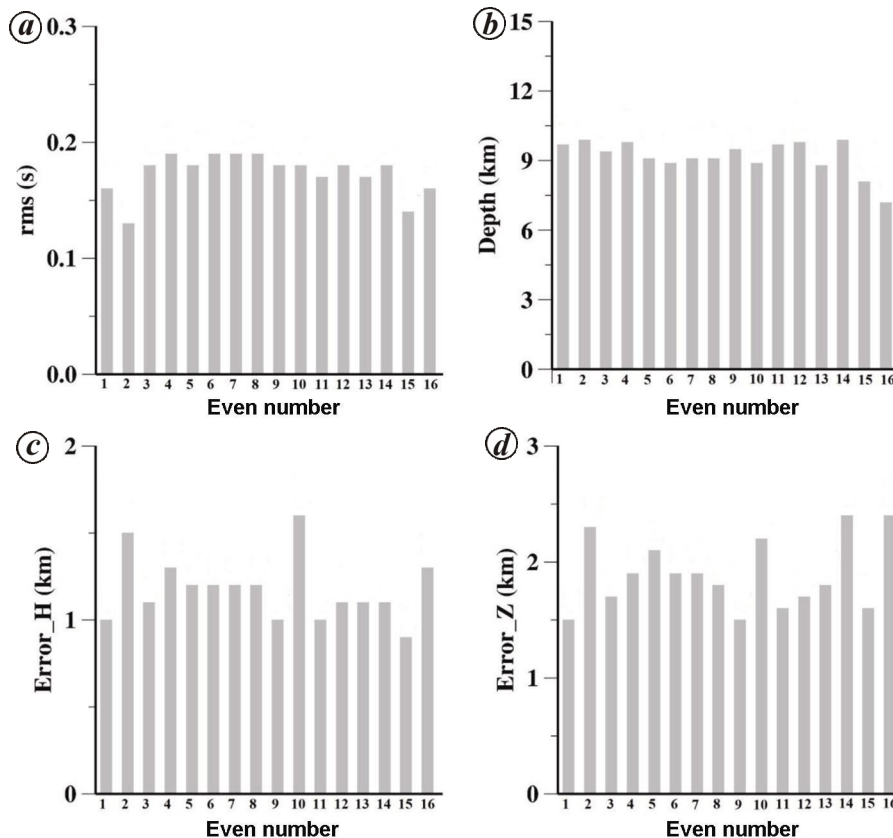


**Figure 5.** Histogram showing (a) rms (sec), (b) focal depth (km), (c) error\_Z (km), (d) error\_H (km) for all the events. The X-axis represents serial number of the events shown in Table 2.

(inset). To assess the depth reliability of these earthquakes, we selected two high-quality earthquakes, each recorded by a minimum of 12 stations with distinct *P*- and *S*-arrivals. In earthquake data analysis, focal depth and origin time occur as a coupled parameter and this leads to their inaccurate estimation from arrival time data. Consequently, we performed a series of inversions for only three free parameters (latitude, longitude and origin time) of the earthquake while keeping its depth fixed in each time (Figure 6). This ensures that depth and origin time are decoupled from each other, and leads to improved global search for focal depth. For a suite of focal depths varying from 1 to 25 km with an increment of 1 km, we computed earthquake location. The solution with minimum rms residual time is finally selected. Results for the two earthquakes are shown in Figure 6, where the variation of rms residual is plotted with depth for different subsets of phase data (combined *P*- and *S*-arrivals and only *P*-arrivals). For the two earthquakes, we have robust estimate of depth, as the rms versus depth function is sharp around the minimum. The minimum misfit is obtained for a depth of 10.0 and 9.0 km. Corresponding inversion result for focal depth is 9.7 and 9.1 km. This sensitivity test confirms that the computed hypocentral depths are reliable.

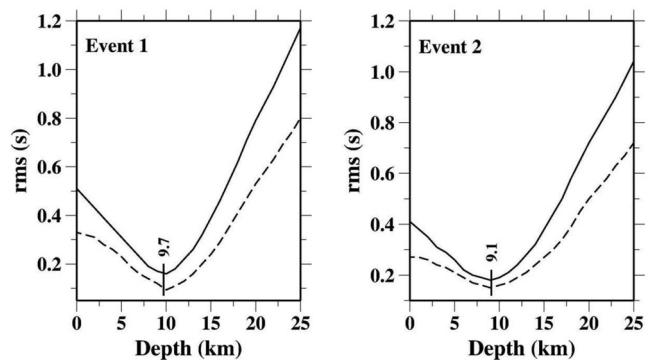


**Figure 6.** Plots of rms versus depth for two earthquakes computed using single-event modelling option. Line styles indicate the subset of arrivals used for location: solid line – all *P* and *S* arrivals and dashed line – all *P* arrivals. Event 1: 26 July 2011, origin time 07:39:16.02, mag. 3.6, 09.745°N 76.905°E. Event 2: 23 August 2011, origin time 13:57:49.29, mag. 1.6, 09.740°N 76.905°E. We also compared the estimated depth with the inversion result (marked vertical line, 9.7 and 9.1 km for events 1 and 2).

The Richter magnitude of an earthquake is determined from the logarithm (log) of the amplitude (*A*) of waves recorded by Wood Anderson seismographs and is given by  $M_L = \log(A/A_0)$ , where  $A_0$  is the amplitude at reference distance. Accordingly, adjustments are included to

**Table 4.** Computed magnitude ( $M_L$ ) of four earthquakes along with those reported by ISC and IMD

Date	UTC (time)	Latitude	Longitude	Present study ( $M_L$ )	ISC ( $M_L$ )	IMD ( $M_L$ )
26/07/2011	07:39:16.02	09.745	76.905	3.6	3.7	3.5
26/07/2011	08:45:55.52	09.752	76.912	2.9	3.2	3.2
18/11/2011	00:15:38.58	09.738	76.915	3.2	3.0	3.1
25/11/2011	21:44:58.34	09.751	76.913	2.9	3.3	3.2

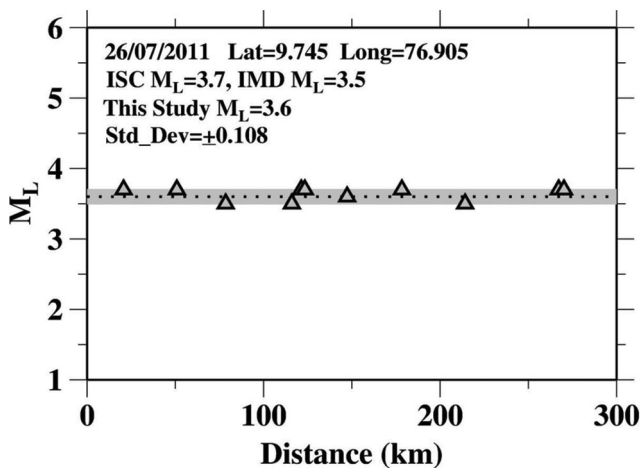


**Figure 7.** Magnitude of an event calculated at 11 different stations with epicentral distances between 17 and 275 km. In this study we used the default calibration functions of the SEISAN software (triangle) based on Alsaker *et al.*<sup>19</sup>. The average of all station is  $M_L = 3.6$  (horizontal dotted line) with a standard deviation of  $\pm 0.108$  (grey area). We also compared our result with the International Seismological Center (ISC) and the India Meteorological Department (IMD) catalogues.

compensate for the variation in the distance between the various seismographs and the epicentre of the earthquake. The magnitudes are determined from the maximum amplitude of the horizontal components. In order to obtain the local magnitude ( $M_L$ ), the seismogram is digitally filtered to simulate the response of Wood Anderson Seismograph and  $M_L$  determined directly from the maximum amplitude of the resulting horizontal seismogram. Final magnitude corresponds to the median value of all individual station magnitudes. Local magnitude ( $M_L$ ) is calculated using the formula<sup>18</sup>

$$M_L = a \times \log(\text{amp}) + b \times \log(\text{dist}) + c \times \text{dist} + d,$$

where amplitude (amp) is the maximum horizontal ground amplitude (zero-peak; nm) of a Wood–Anderson simulation of the recorded seismogram, and dist is the hypocentral distance (km). We used calibration parameters ( $a$ ,  $b$ ,  $c$ ,  $d$ ) provided by Alsaker *et al.*<sup>19</sup>, where  $a = 1.0$ ,  $b = 0.91$ ,  $c = 0.00087$  and  $d = 1.67$ . To establish the suitability of the calibration constants with geology of the region and to correct for the attenuation parameter, we computed magnitude as a function of distance (Figure 7). We observed that the magnitude did not deviate

significantly with the epicentral distance (standard deviation  $\sim \pm 0.108$ ). Absence of any systematic distance dependence of the calculated magnitude suggests that the calibration parameter<sup>19</sup> is an appropriate description of the attenuation in this region. We compare in Table 4, parameters of four earthquakes determined in this study with those computed by the International Seismological Center (ISC) and the India Meteorological Department (IMD). Our computed magnitude for the earthquakes is close to those determined using ISC and IMD catalogues. As an example we show the result for an event (Figure 7), which shows no significant deviation from the magnitudes calculated with the help of default parameters of SEISAN. Using the stated parameters, we computed magnitude of all the 16 earthquakes (Table 2).

We computed focal mechanism solution of six well-recorded earthquakes having clear  $P$ -wave first motion and azimuthal gap  $< 125^\circ$  using the program FFPIT<sup>20</sup>, a grid search routine that minimizes the misfit between nodal planes and the observed first motion data. For each of these earthquakes we used 12–16  $P$ -wave first motions, manually picked on the raw seismogram. These earthquakes have magnitudes varying from 2 to 3.6. In Figure 8, the  $P$ -wave first motions are plotted on the lower hemisphere of an equal area projection for the largest magnitude event ( $M_L = 3.6$ ). The focal mechanism solutions are shown in Figure 9 and listed in Table 5. Faulting types are calculated following the convention of Aki and Richards<sup>21</sup>. Because these classifications are based on the rake angle, it is necessary to fix the fault plane between the two nodal planes using the geological information. All the focal mechanism solutions have similar faulting character, regardless of which nodal plane is assumed to be the fault plane. The nodal planes of focal mechanism solutions show NW–SE and NE–SW direction indicating strike-slip faulting. These solutions suggest that the movement is right-lateral strike-slip along the NW–SE plane, and is considered to be the fault plane, also corroborated from geological evidence. Our results agree with the causative nodal plane of the composite focal mechanism solution by Rastogi *et al.*<sup>7</sup>. This focal mechanism solution displays average strike-slip faulting with right-lateral movement and the  $P$ -axis is nearly vertical, while the  $T$ -axis is almost sub horizontal.

Scientific opinion is divided on the causative source for the Idukki earthquakes: tectonic or the reservoir

**Table 5.** Calculated parameter for fault plane solutions, where NP1 and NP2 represent the first and second nodal planes

Date	UTC (time)	Magnitude ( $M_L$ )	Depth (km)	Strike NP1	Dip NP1	Rake NP1	Strike NP2	Dip NP2	Rake NP2
26/07/2011	07:39:16.02	3.6	9.7	317.00	48.50	-172.86	222.26	84.66	-41.72
26/07/2011	10:56:43.21	2.4	9.4	315.78	61.42	-153.81	212.54	67.20	-31.26
17/09/2011	22:26:24.40	2.0	8.9	332.66	82.22	-146.80	237.60	57.14	-09.27
17/11/2011	23:57:57.15	2.6	9.7	326.32	59.01	-168.07	230.11	79.79	-31.55
18/11/2011	00:15:38.58	3.2	9.8	324.73	79.54	-165.27	232.00	75.52	-10.81
25/11/2011	21:44:58.34	2.9	8.8	316.59	72.99	-162.82	221.42	73.59	-17.76

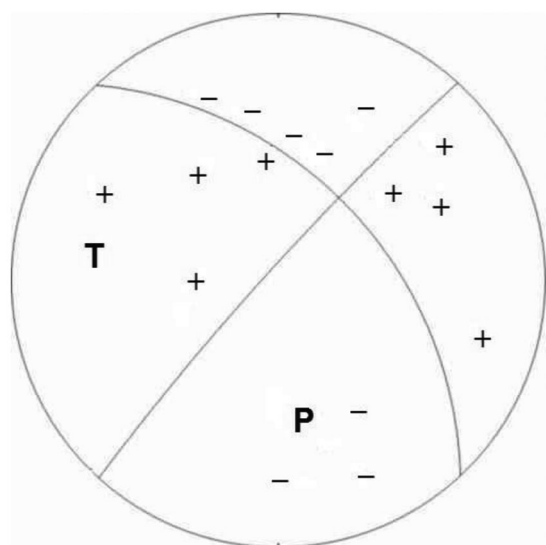


**Figure 8.** Example of one focal mechanism solution obtained from 16 first *P*-motion data using FPFIT program. We used data from seismograph station with two symbols: a minus (-) if the *P*-wave first motion is down, a plus (+) if the first motion is up.

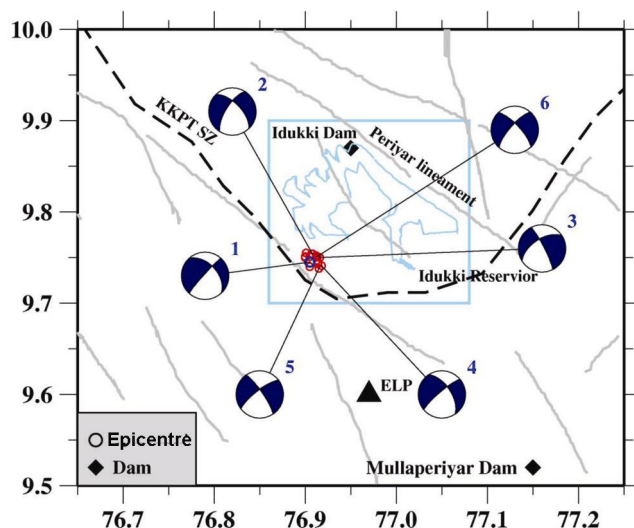


**Figure 9.** Area around the Idukki Reservoir showing faults and lineation (after Rajendran *et al.*<sup>5</sup>) with focal mechanism solutions. The events are numbered in chronological order, with details in Table 5. The focal mechanism solution, numbered 1, represents the main event ( $M_L = 3.6$ ).

triggered (RTS). We discuss below certain characteristics of these two to understand the nature of earthquakes and also to differentiate between them.

(i) Global review of RTS suggests no known example that has occurred beyond a period of two decades after initial impoundment<sup>22</sup>. The recent seismicity near Idukki that occurred nearly 35 years after the initial burst of activity in 1977, could therefore be a doubtful case of RTS.

(ii) Weekly change in the lake water level and frequency of tremors during 2007–2011 suggest no significant change in any of these parameters during the five years<sup>3</sup>. Also, earthquake activity does not appear to be associated with the rate of reservoir filling or rainfall intensity. So we cannot correlate this seismic activity with the reservoir effect.

(iii) The change of stress that may weaken a fault due to lake water level changes responsible for generating RTS has been an issue of prolonged debate. Current knowledge suggests that water level changes of 1–1.5 m/week lead to stress changes by ~0.1 bar or less at the shallow seismogenic depth (2–5 km)<sup>23,24</sup>. This is generally applicable to most RTS. Since the recent

earthquakes in Idukki region have focal depth of 9–10 km, their occurrence cannot be related with the change of lake water level.

(iv) In the case of RTS, generally foreshock activity precedes the main event<sup>6</sup>. No such observation is reported in this case.

(v) The earthquake focal mechanism computed by us is strike-slip with right lateral movement, as also reported by Rastogi *et al.*<sup>7</sup> for 1988 Idukki earthquake. The earthquake epicentres are closely related to a NW–SE trending fault associated with the KKPT shear zone, suggesting a genetic linkage between them.

We investigated location and mechanics of 16 small earthquakes ( $M_L$  1.5–3.6) that occurred near the southwest part of Idukki Reservoir, Kerala. These are recorded on a network of 21 temporary seismic stations during January 2011–March 2012. With these adequate number of seismic stations, we present accurate hypocentre location and fault plane solutions of these events. These earthquakes have focal depth of 7.2–9.9 km and are unlikely to be triggered by the stress generated due to reservoir loading that usually supports earthquakes at

shallow depth (<5 km). This is further supported by absence of foreshock activity and no clear correlation with water-level time series.

The recent earthquakes are confined along NW–SE trending faults and KKPT shear zone, about 6–8 km southwest of Idukki Reservoir. The fault plane solution is derived for six events using clear first-motion *P*-waves. The calculated fault plane solutions suggest strike-slip faulting with right-lateral movement along a NW–SE trending nodal plane; *P*-axis being nearly vertical along N–S direction and *T*-axis almost sub-horizontal (E–W direction). The Idukki region is traversed by several major lineaments and faults, the Periyar and KKPT being the major lineaments in the study region. The lineaments represent major shear zones<sup>14,15</sup>. The lineament fabric of the region shows a predominance of NW–SE and NE–SW trending fault sets, as also supported by focal mechanism solutions. Review of historical as well as recent seismicity records and the results from fault plane solutions for the region, suggest that the NW–SE trending faults and the KKPT shear zone in central Kerala could be a potential region for future low to moderate magnitude earthquakes.

1. Rai, S. S. *et al.*, South India Precambrian crust and shallow lithospheric mantle: initial result from the India Deep Earth Imaging Experiment (INDEX). *J. Earth Syst. Sci.*, 2013, **122**, 1435–1453.
2. Paul, J. *et al.*, Stability of Peninsular India 1864–1994. *Proc. Indian Acad. Sci. (Earth Planet. Sci.)*, 1995, **104**, 131–146.
3. Rajendran, K., Rajendran, C. P., Kesavan, S. and Naveen, R., Recent micro tremors near the Idukki Reservoir, Kerala, South India. *Curr. Sci.*, 2012, **102**, 1446–1451.
4. Padale, J. G. and Das, P. B., A note on the recent seismic activity in the Idukki District, Kerala. Report, Central Water and Power Research Station, Pune, 1988, p. 12.
5. Rajendran, C. P., John, B., Sreekumari, K. and Rajendran, K., Reassessing the earthquake hazard in Kerala based on the historical and current seismicity. *J. Geol. Soc. India*, 2009, **73**, 785–802.
6. Singh, H. N., Raghavan, V. and Varma, A. K., Investigation of Idukki earthquake sequence of 7th–8th June. *J. Geol. Soc. India*, 1989, **34**, 133–146.
7. Rastogi, B. K., Chadha, R. K. and Sarma, C. S. P., Investigations of June 7, 1988 earthquake of magnitude 4.5 near Idukki dam in Southern India. *Pure Appl. Geophys.*, 1995, **145**, 109–122.
8. Rajendran, K. and Rajendran, C. P., Low–moderate seismicity in the vicinity of Palghat Gap, South India, and its implications. *Curr. Sci.*, 1996, **70**, 303–307.
9. Rastogi, B. K., Erattupettah earthquake of 12 December 2000 and seismicity of Kerala. *J. Geol. Soc. India*, 2001, **57**, 27–274.
10. Bhattacharya, S. N. and Dattatrayam, R. S., Earthquake sequence in Kerala during December 2000 and January 2001. *Curr. Sci.*, 2002, **82**, 1275–1278.
11. Guha, S. K., Padale, J. G. and Gosavi, P. D., Probable risk estimation due to reservoir-induced seismicity. In *Dams and Earthquakes*, Institution of Civil Engineers, London, 1981, pp. 297–305.
12. Harendranath, L., Rao, K. C. B., Balachandran, V. and Rajagopal, G., Recent significant earthquakes in quick succession in Kottayam Idukki region, Kerala – a macroseismic study. *J. Eng. Geol.*, 2005, **32**, 31–35.
13. Rajendran, K., John, B. and Rajendran, C. P., Report on the microseismic activity around Idukki and Idamalayar reservoirs, for the period July–September 1997. Report submitted to KSEB, Government of Kerala, 1999, p. 11.
14. Rao, P. S., Some aspects of structure and tectonics of Kerala region, India and related mineralization. *Geol. Surv. India*, 1978, **19**(3), p. 53.
15. Katz, M. B., Tectonic evolution of Archean granulites facies belt of Sri Lanka–South India. *J. Geol. Soc. India*, 1978, **19**(5), 185–205.
16. Haskov, J. and Ottermoller, L., SEISAN: the earthquake analysis software, version 8.1.1. Institute of Solid Earth Physics, University of Bergen, Norway, 2013.
17. Lineart, B. R. E. and Havskov, J., A computer program for locating earthquakes both locally and globally. *Seismol. Res. Lett.*, 1995, **66**, 26–36.
18. Hutton, L. K. and Boore, D. M., The ML scale in southern California. *Bull. Seismol. Soc. Am.*, 1987, **77**, 2074–2094.
19. Alsaker, A., Kvamme, L. B., Hansen, R. A. and Dahle, A., The  $M_L$  scale in Norway. *Bull. Seismol. Soc. Am.*, 1991, **81**, 379–398.
20. Reasenber, P. A. and Oppenheimer, D., FPFIT, FPLOT and FPPAGE; Fortran computer programs for calculating and displaying earthquake fault plane solution. US Geological Survey Report, Open-File Report, 1985, pp. 85–739.
21. Aki, K. and Richards, P. G., *Quantitative Seismology*, W.H. Freeman, New York, 1965.
22. Rajendran, K., Thulasiramanand, K. and Sreekumari, K., Microearthquake activity near the Idukki Reservoir, South India: a rare example of renewed triggered seismicity. *Eng. Geol.*, 2013, **153**, 45–52.
23. Rajendran, K., Sensitivity of a seismically active reservoir to low-amplitude fluctuations: observations from Lake Jocassee, South Carolina. *Pure Appl. Geophys.*, 1995, **145**, 87–95.
24. Deng, K., Zhou, S., Wang, R., Robinson, R., Zhao, C. and Cheng, W., Evidence that the 2008  $M_w$  7.9 Wenchuan earthquake could not have been induced by the Zipingpu Reservoir. *Bull. Seismol. Soc. Am. B*, 2010, **100**, 2805–2814.

ACKNOWLEDGEMENTS. Seismograms used in this study are collected from broadband seismic stations operated by the CSIR–NGRI. We thank Ritima Das for providing inversion results of receiver function. This is a part of the PhD work of Utpal Saikia. All the figures were generated using Generic Mapping Tools version 4.5.0 ([www.soest.hawaii.edu/gmt](http://www.soest.hawaii.edu/gmt)). S.S.R. is supported by J.C. Bose national fellowship.

Received 22 April 2014; revised accepted 5 September 2014